



**HAL**  
open science

## Plastic foil micro-grooved by embossing enhances dew collection without aging effects

Nicolas Lavielle, Anne Mongruel, Tarik Bourouina, Laurent Royon, Daniel Beysens

► **To cite this version:**

Nicolas Lavielle, Anne Mongruel, Tarik Bourouina, Laurent Royon, Daniel Beysens. Plastic foil micro-grooved by embossing enhances dew collection without aging effects. *Materials Today Sustainability*, 2023, pp.100566. 10.1016/j.mtsust.2023.100566 . hal-04262944

**HAL Id: hal-04262944**

<https://hal.sorbonne-universite.fr/hal-04262944v1>

Submitted on 27 Oct 2023

**HAL** is a multi-disciplinary open access archive for the deposit and dissemination of scientific research documents, whether they are published or not. The documents may come from teaching and research institutions in France or abroad, or from public or private research centers.

L'archive ouverte pluridisciplinaire **HAL**, est destinée au dépôt et à la diffusion de documents scientifiques de niveau recherche, publiés ou non, émanant des établissements d'enseignement et de recherche français ou étrangers, des laboratoires publics ou privés.

# Plastic foil micro-grooved by embossing enhances dew collection without aging effects

Nicolas Lavielle<sup>1,2</sup>, Anne Mongruel<sup>1</sup>, Tarik Bourouina<sup>2,3</sup>, Laurent Royon<sup>4</sup>, Daniel Beysens<sup>1,5</sup>

- (1) Physique et Mécanique des Milieux Hétérogènes, CNRS, ESPCI, PSL Research University, Sorbonne Université, Université Paris Cité, 75005 Paris, France
- (2) ESYCOM lab, UMR 9007 CNRS, Univ Gustave Eiffel, 77454 Marne-la-Vallée, France
- (3) CINTRA, IRL 3288 CNRS-NTU-THALES, Nanyang Technological University, 637553, Singapore
- (4) Laboratoire des Energies de Demain, Université Paris Cité, UMR 8236 CNRS, Paris, 75013, France
- (5) OPUR, Paris, France

## Abstract:

Low-tech, radiative and recyclable plastic foil is considered for the passive collection of dew water. Fashioning micro-grooves at its surface by hot embossing improves by a large factor the collection of even tiny water drops. We show that this improvement is conserved under harsh outdoor conditions. The ability of the micro-grooved foil to collect condensed water is measured by the latency time  $t_l$  to collect the first drop at the bottom of a vertical substrate. Compared to the same, smooth foil,  $t_l$  is smaller for the micro-grooved foil by an order of magnitude. Under severe outdoor conditions (dust storm, heat wave) the properties of the micro-grooved foil are preserved after 6 months whereas the collection properties of the smooth foil have decreased by 50%. The basic reason is the insensitivity of the water collection mode to the evolution of the surface wetting and roughness properties. Such low cost, scalable and robust material should find applications in passive water harvesting devices to supply supplementary fresh water in regions where water is, or is becoming, a scarce resource.

## Keywords:

Dew water, dropwise condensation, micro-grooves, surface aging, outdoor aging, collection rate, radiative cooling, water harvesting.

## Introduction:

In the context of global warming, fresh water availability is becoming a global challenge<sup>1</sup>. Water accessibility now affects other regions than arid or semi-arid regions, especially during the hot summer season. Since the atmosphere contains a large amount of water vapour ( $1,3 \times 10^{13} \text{ m}^3$ )<sup>2</sup>, efforts have been recently made to harvest atmospheric water vapour using active or passive collectors as a supplementary source of fresh water<sup>3</sup>. The design of atmospheric

condensers is concerned with the three following physics domains. (i) Thermal processes. In order to achieve water condensation, active or passive collectors must cool the collecting surface below the dew point temperature of the surrounding air. Passive systems avoid the use of energy supply and lower the production cost but their yield is limited by the available radiative deficit (lower than  $100 \text{ W.m}^{-2}$ ), the heat exchange with the surrounding air (heat exchange coefficient  $2\text{-}8 \text{ W.m}^{-2}\text{.K}^{-1}$ ) and the high value of the latent heat of water ( $2500 \text{ kJ/kg}$ )<sup>4</sup>. In the most favourable case where the dew point temperature is close to the ambient temperature (this happens at night for a relative humidity of air close to 100%) this radiative deficit is used principally for the phase change, yielding a maximum on order 1 litre of dew water per square meter per night<sup>4</sup>. Yields as large as  $0.8 \text{ L.m}^{-2}\text{.night}^{-1}$  have indeed been reported<sup>5</sup>. (ii) Wetting characteristics. Surface properties can lead to dropwise or filmwise condensation. Dropwise condensation, when active cooling is used, is preferred to avoid the thermal insulation inherent to the presence of a water layer formed by filmwise condensation, which decreases condensation rate and lowers the heat transfer by an order of magnitude<sup>6</sup>. This limitation does not apply to passive condensers where the condensed water surface is also cooled by radiation deficit. (iii) Adhesion. In the case of dropwise condensation (the most general case outside because of fatty acid pollution), the ability of the condensing surface to rapidly remove and collect the condensed water by gravity is crucial. It is the case in active system where the shedding of the largest drops determines the thermal efficiency and the ability to induce re-nucleation to achieve higher condensation rates<sup>7</sup>, and also in passive devices to avoid evaporation upon sunrise<sup>4</sup>. Surfaces with low water contact angle hysteresis (small drop pinning forces) are thus looked for. In addition, the condensing surfaces should be sustainable and robust to maintain its properties under severe weather conditions (UV, rain, wind or dust abrasion and deposition). However, aging issues could severely compromise the expected thermal, wetting or pinning properties. Low hysteresis surfaces, such as superhydrophobic surfaces or liquid-infused surfaces might fail upon aging. Robust superhydrophobic surfaces<sup>8</sup> have been recently engineered to overcome the deterioration of surface structures. Strategies have been found to avoid in liquid-infused surfaces the oil depletion<sup>9,10</sup>. Aging of other novel and promising surfaces such as bio-inspired, fluid-manipulating surfaces<sup>11,12</sup> or biphilic patterned surfaces<sup>13-16</sup> should be investigated since their surface properties might evolve with time.

In this context, we present here a study of a micro-grooved low density polyethylene upgraded foil surface ( $\mu$ -foil). It is a potential surface for condensing and efficiently collecting atmospheric water vapour while remaining insensitive to aging. In order to initiate water condensation, microbeads of  $\text{TiO}_2$  and  $\text{BaSO}_4$  are embedded in the  $\mu$ -foil material in order to increase the emissivity in the atmospheric window and reflect the sun light<sup>17</sup>. High thermal emittance (hemispherical emissivity  $\sim 0.94$ ; in the atmospheric window) enables a negative IR radiative exchange with the atmosphere that lowers the surface temperature<sup>18</sup> to initiate water condensation. When wet, the mean surface emissivity is close to water emissivity ( $0.95$ ;  $0.98$  in the atmospheric window)<sup>19</sup>. The solar reflectance of the material ( $0.84$ )<sup>17</sup> limits surface heating when exposed to sun light. This passive material takes advantage of radiative cooling,

while keeping a cost production on the order of one euro per square meter. Regarding wetting and water pinning properties, a water insoluble food-proof surfactant was also added. It migrates at the surface and promote rapid droplet shedding. The foil used was manufactured by OPUR and its thickness was 300  $\mu\text{m}$ . Micro-grooves (width, spacing, depth,  $w = s = d = 50 \mu\text{m}$ ) were engineered on the surface of the foil by using the hot embossing method, which is scalable on large surfaces. Micro-grooved surfaces have been shown to collect condensing water in an efficient manner, by enhancing the growth of some droplets and their shedding by gravity<sup>20</sup>. Droplets condense on the plateaus and coalesce with the channels filled with condensed water. These channels then supply with water the droplets that form at the bottom of the collecting surface<sup>21</sup>. More complex re-entrant grooves have even been recently engineered to take advantage of this fashion to collect water, they avoid flooding and an increase of the water collection rate was indeed measured<sup>22</sup>.

In this work we compare the ability of  $\mu$ -foil and smooth foil (s-foil, with same composition as the  $\mu$ -foil but without grooves) to collect water in a climatic chamber prior aging under various climatic conditions and after being exposed to outdoor aging. The surfaces were placed on a 30° tilted planar support oriented SW on a terrace, about 20 m elevation, in Paris (5<sup>th</sup> arrondissement). A tilt of 30° was imposed because this angle provides the optimal balance between atmospheric radiative exchange and gravity-assisted shedding<sup>4</sup>. The overall test duration was 6 months, between 17/02/2022 and 17/08/2022. Outside temperatures were measured between 0.2°C and 39.7°C, with several heat waves. The wind speed was measured between 0 and 20.5 m/s, with several episodes of storm, of which one “sandstorm”, with intense rain and wind full of grains from the Sahara Desert. The smooth and micro-grooved foils were periodically tested, initially before being positioned outside, then after one week (1 W), one month (1 M), three months (3 M) and 6 months (6 M). The tests consisted in condensation and collection in a vertical position in a climatic chamber, water was collected at the bottom of the plate by a hydrophilic tissue placed at 0.1 mm from the surface and connected to a balance. Two parameters were deduced from the evolution of the collected mass: (i) The latency time  $t_l$  for first droplets collection at the bottom of the substrate and (ii) the water collection rate. The main result is concerned with the ability of micro-grooved foil to maintain its enhanced water collection characteristics with ageing thanks to the micro-patterning. Compared to s-foil, after 6 months aging,  $\mu$ -foil exhibits almost an order of magnitude smaller  $t_l$  for droplet collection while increasing by 50% the water collection rate.

## **Results and discussion:**

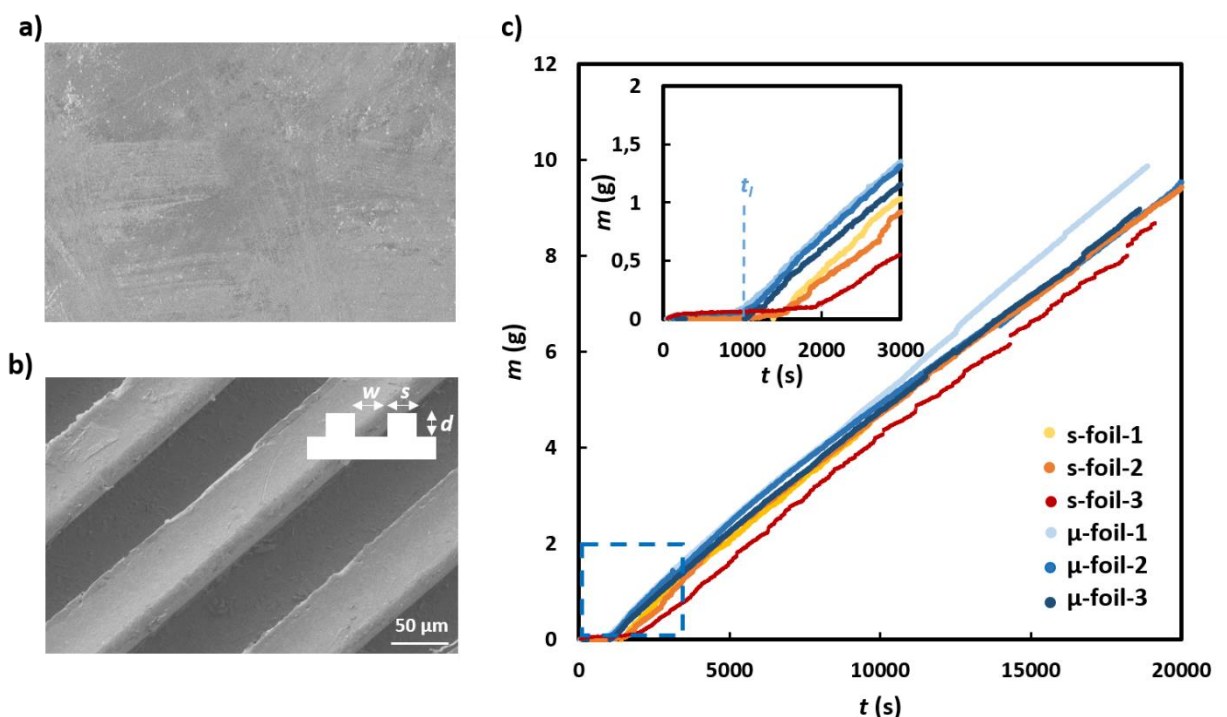
### **Water collection repeatability:**

Both s-foil and  $\mu$ -foil samples ( $9 \times 9 \text{ cm}^2$ ) were tested in a climatic chamber under given climatic conditions (30°C, 70% RH, vapour pressure  $\sim 3.0 \text{ kPa}$ ) during 4 hours, with a surface temperature set at 16°C (saturation vapour pressure  $\sim 1.8 \text{ kPa}$ ). In these conditions, the

supersaturation is  $\sim 1.7$  and the dew point temperature is  $23.5^{\circ}\text{C}$ . Movie S1 compares the s-foil and  $\mu$ -foil under these condensation experiments prior setting the surfaces outdoor. One observes a striking difference between the two samples under the same operating conditions: For s-foil, discrete droplets are formed and shedding of the droplets takes place with coalescence with other droplets leading to rivulets. In contrast, with  $\mu$ -foil the filling of the grooves is firstly observed, then accompanied by the formation of major droplets directly at the bottom of the sample. One also observes that the beginning of water collection at  $t_l$  happens faster for the  $\mu$ -foil sample. Indeed the micro-grooves in the  $\mu$ -foil sample fundamentally modify the growth and coalescence of water droplets<sup>20,21</sup> On the s-foil, the nucleation of droplets is followed by their growth by diffusion and coalescence with neighbors' droplets. They eventually reach a critical size where the gravitational forces overcome the pinning forces, leading to droplet shedding. In contrast, for the  $\mu$ -foil, the presence of the micro-grooves drastically changes the collection mode of the condensed water. On the plateaus is present a continuous process of nucleation, growth and coalescence of droplets that soon coalesce with the grooves filled with water. The grooves then continuously supply water to major droplets present at the bottom of the sample. A detailed description of this process is given in Refs. 20,21.

Condensation on both s- and  $\mu$ -foil substrates was performed three times each to assess the repeatability with condensation lasting 4 hours each. Figure 1a and 1b presents the surface morphology of s-foil and  $\mu$ -foil, respectively. Figure 1c gives the evolution of the collected mass for the two samples during the three tests. In addition, the three condensation cycles also aimed to verify the constancy of collection ability after several condensation processes. The inset in Figure 1c focuses on short times (the first 3000 s of the experiment). Concerning the s-foil, one observes a small increase of the latency time  $t_l$  from experiment 1 to experiment 2 and a larger increase from experiment 2 to experiment 3, making  $t_l$  to gradually increase from 1500 s to 2000 s. Such increasing delay is not observed with the  $\mu$ -foil where the latency times do not change. Figure 1c exhibits similar slopes  $dm/dt$  for the 6 experiments, which indicates that the condensation rates were indeed similar for all experiments. One however notes some experimental variations, especially with the  $\mu$ foil-1 which exhibits at large times ( $t > 10,000$  s) a somewhat larger slope. The steady state of condensation is controlled by only the available cooling power and the supersaturation. All s- and  $\mu$ -foils should therefore exhibit the same condensation rates  $dm/dt$  in the steady state, the observed difference being attributed to the variations between the experiments of either the cooling power, which can vary with the thermal resistance of the drops, and the supersaturation. For the s-foil, the increase of the latency times corresponds to an increase of the critical shedding drop size. This increase does not appreciably affect the slope  $dm/dt$ , which means that the thermal resistance of such small drops can be neglected. It is all the more true for the  $\mu$ -foil where the largest drop diameter is at most the half-thickness of the groove plateaus, that is  $25\ \mu\text{m}$ . The somewhat larger condensation rate of run  $\mu$ -foil1 is thus due to a variation in the experimental supersaturation.

The increase of the shedding latency time for the s-foil with the number of the condensation runs indicates that the shedding properties were somewhat altered with the condensation cycles. We tentatively interpret this evolution by a weak diminution of the surface surfactant with the number of experiments, increasing the pinning forces as measured by the contact angle hysteresis (CAH) and therefore the critical drop size for shedding, proportional to  $CAH^{23}$ , and thus the shedding latency time. Concerning the  $\mu$ -foil sample, no significant difference is observed in Figure 1c between the 3 experiments before 12000 s. Later, the run s-foil1 exhibits a somewhat larger condensation rate that can be attributed to the variations of supersaturation. The latency time does not vary because the efficiency of collection is not related to a critical value of the drop pinning forces but to a process involving the groove geometry.

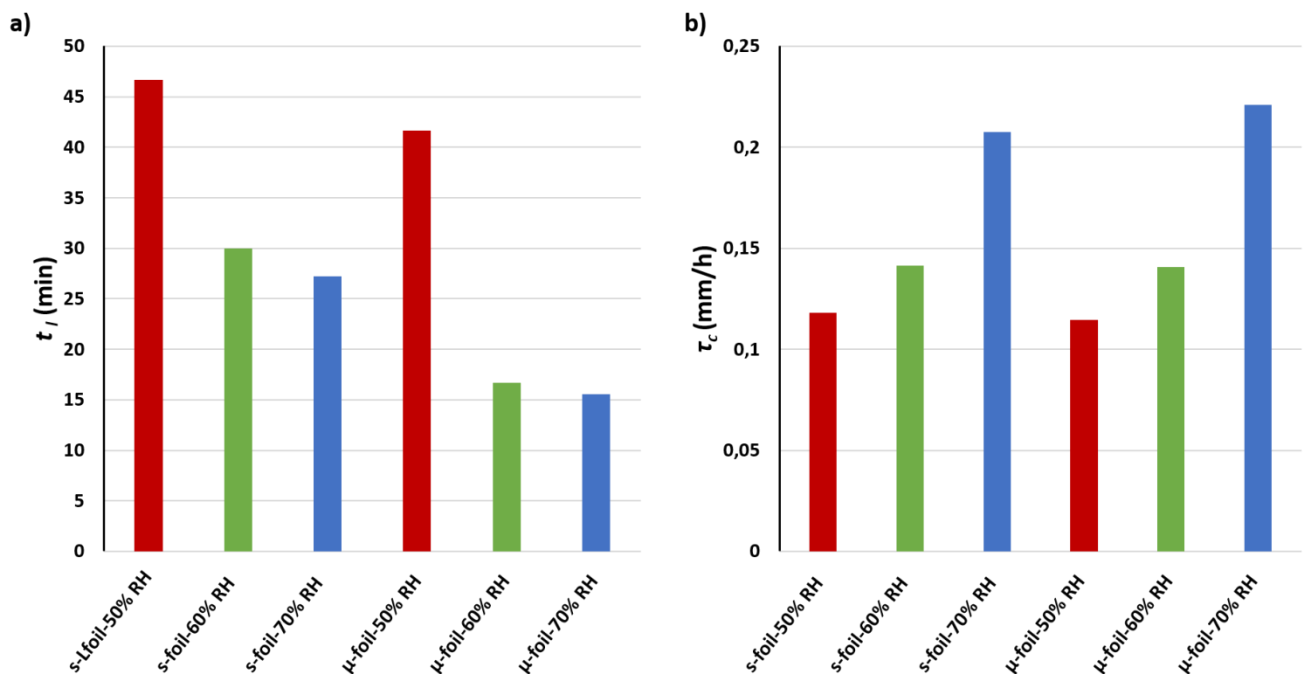


**Figure 1: Foil surface morphologies and water collection repeatability:** (a) Scanning electron microscope images of the surface morphology of s-foil (a) and  $\mu$ -foil (b). (c) Evolution of the mass of the collected water of triplicates condensation experiments for s-foil and  $\mu$ -foil. The inset focuses on the first 3000 s. The latency time,  $t_l$ , represents the time needed to collect the first droplets.

#### Water collection under various climatic conditions:

To further explore the potential of  $\mu$ -foil to harvest condensed water, the samples were placed, without prior outdoor aging, in the climatic chamber under various condensation conditions to mimic various climatic conditions. The collected mass of water was monitored with time. The temperature of the chamber was set at 30°C, the temperature of the sample at 16°C, and the varying parameter was the relative humidity (RH) set at 50, 60 and 70 %. The

dew point temperature in these conditions was respectively 17.5, 21.0 and 23.5 °C. These different condensation conditions correspond to temperature supersaturations of 1.5 °C, 5°C and 7.5°C. In Figures 2a and 2b are shown the latency time and the collection rate for both the s- and  $\mu$ -foils as a function of RH. One observes that for any condensation conditions,  $t_l$  is markedly smaller for the  $\mu$ -foil as compared to the s-foil, with a larger decrease when RH increases. This difference can be attributed to the time needed to fill the micro-channels ( $t_f$ ), a decrease of the condensation rate leads to an increase of  $t_f$  and thus of  $t_l$ . Regarding the collection rate, no significant difference is observed between the s-foil and  $\mu$ -foil samples. This is because, in the steady state of condensation, only matters the available cooling flux, which is the same for both s- and  $\mu$ -foils when the droplet critical shedding size remains small. Nevertheless, after aging, this critical size increases and condensation of s-foil becomes weaker than with  $\mu$ -foil. This thermal effect should not occur under outdoor radiative cooling where water cools very efficiently due to its high emissivity.



**Figure 2: Water collection capability under various climatic conditions for s-foil and  $\mu$ -foil:** (a) Latency time for first droplet collection,  $t_l$ , in min. at 50, 60 and 70% relative humidity. (b) Collection rate,  $\tau_c$ , expressed in volume of the collected water per surface area and time at 50, 60 and 70% relative humidity. Temperature of the sample: 16°C, air temperature: 30°C.

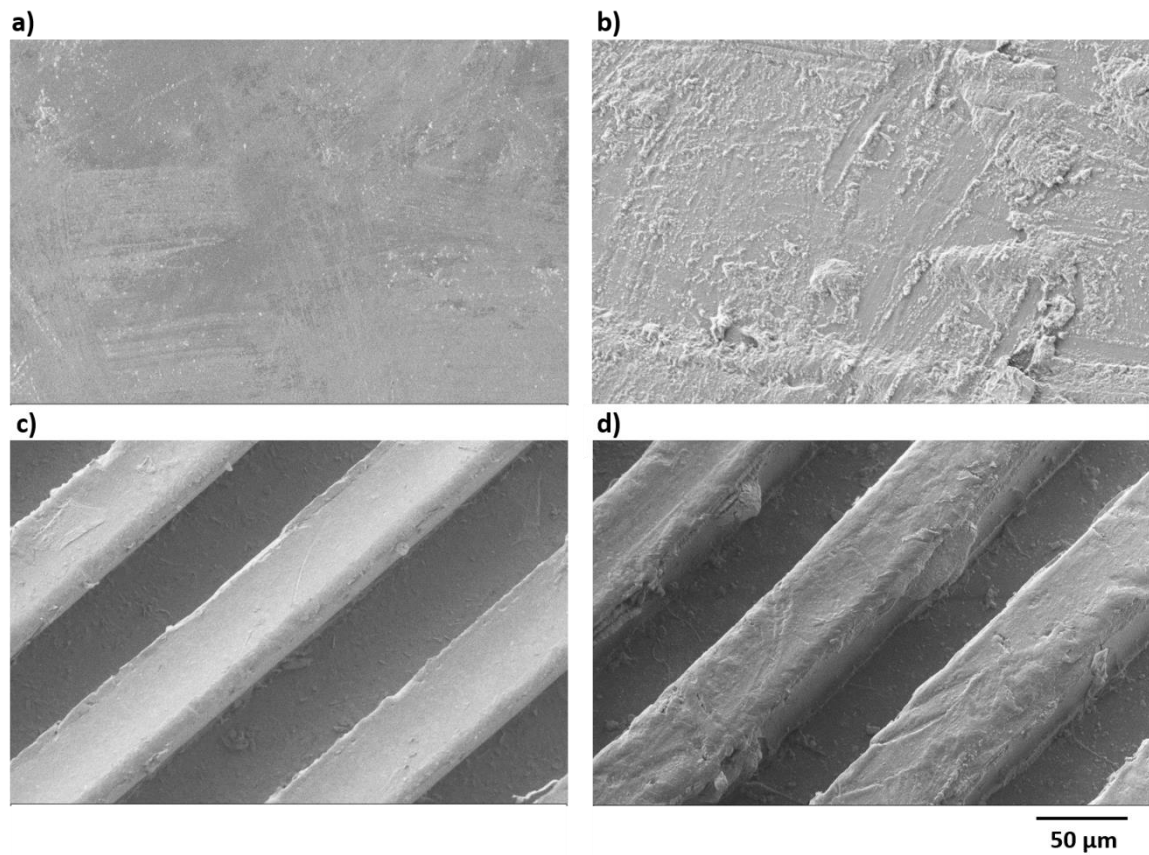
#### Water collection and outdoor aging:

Once the condensation repeatability and water collection under various climatic conditions were studied, the two s- and  $\mu$ -foil samples were placed outdoor. The samples were tested under the same experimental conditions of Figure 1 in the climatic chamber at different aging


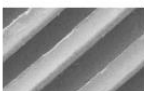


times: 1 week (1 W), 1 month (1 M), 3 months (3 M) and 6 months (6 M). Figure 3 presents the surface morphology of the s-foil and  $\mu$ -foil samples before aging (a, c) and after 6 months aging (b, d). One can observe a deterioration of the surface morphology with aging, the surface roughness increasing for both samples. This phenomenon leads to an apparent weak swelling of the structures. The morphology evolution is due to dust deposition, surface abrasion (dust, wind, rain) and solar exposure (heat, UV). This surface deterioration should impact the water collection ability of the samples under study. Regarding the evolution of the radiative properties of s-foil and  $\mu$ -foil, table 1 presents the normal emissivity, hemispherical emissivity and albedo before aging and after 6 months aging. Normal directional and the hemispherical emissivity are obtained with the EM3 emissiometer from THEMACS Engineering at room temperature (288K) (cf. details of the measurement in Supplementary Information). The spectral reflectance (from 250nm to 2500 nm) carried out using a Cary 5000 UV/Vis/NIR spectrophotometer, is averaged over the standard AM 1.5G solar spectrum from ASTM E903 (ASTM International, 2012) to obtain an approximate value of albedo.

The introduction of the micro-grooves to the  $\mu$ -foil slightly increases the hemispherical emissivity from 0.92 to 0.94. and decreases the albedo from around only 2%. After 6 months aging, one notices that there is no significant evolution of the IR emissivity of both foils, which indicates that the cooling ability of the foils should not be impacted with outdoor aging. About visible-near IR radiation that is reflected by the foil., the albedo shows a decrease for  $\mu$ -foil only ( $\approx$  6% decrease), which confirms that this parameter is highly sensitive to the surface properties of the foil.





**Figure 3: Surface morphology evolution with outdoor aging:** Scanning electron microscope images of the surface morphology of s-foil and  $\mu$ -foil before (a, c) and after 6 months aging (b, d).

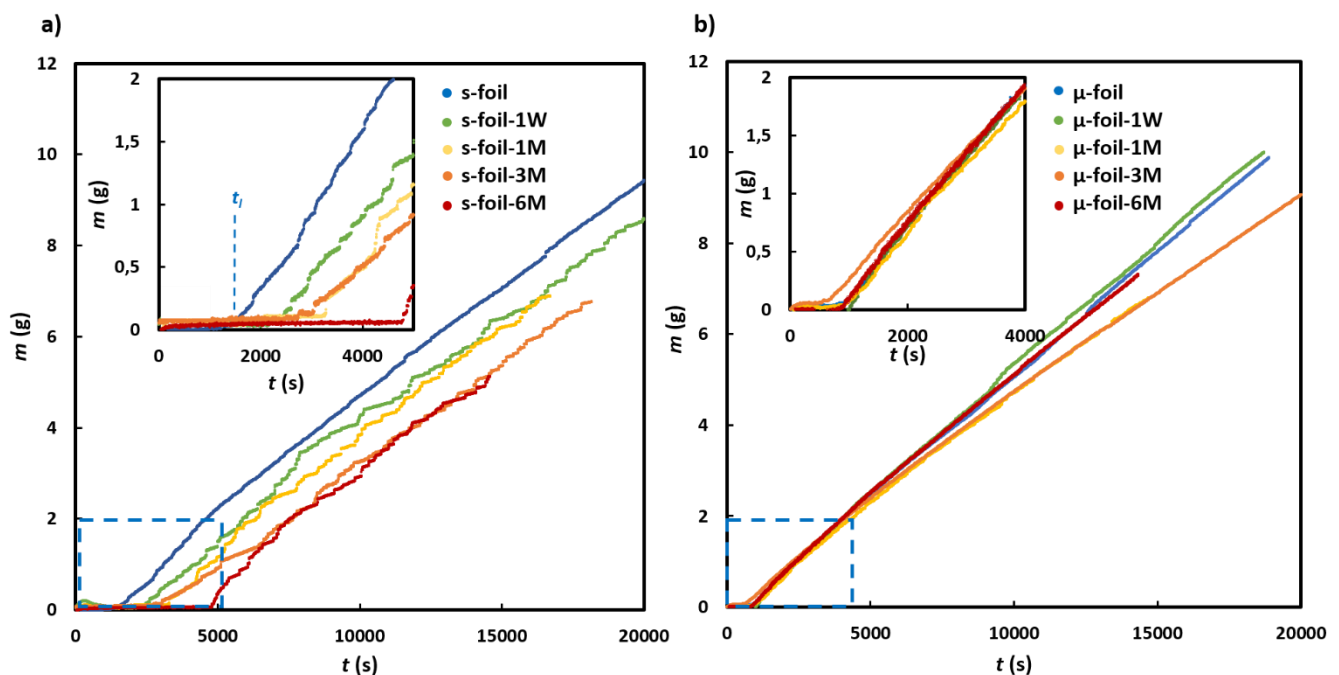
	SEM image	Normal emissivity	Hemispherical emissivity	Albedo
s-foil		$0.960 \pm 0.003$	$0.916 \pm 0.004$	$0.758 \pm 0.001$
$\mu$ -foil		$0.967 \pm 0.006$	$0.941 \pm 0.010$	$0.743 \pm 0.001$
s-foil-6M		$0.947 \pm 0.002$	$0.912 \pm 0.003$	$0.756 \pm 0.001$
$\mu$ -foil-6M		$0.965 \pm 0.003$	$0.939 \pm 0.005$	$0.701 \pm 0.001$

**Table 1: Normal emissivity, hemispherical emissivity and solar reflectivity (albedo) of s-foil and  $\mu$ -foil before aging and after 6 months (6M) outdoor aging.**

**s-foil study.** The movie S2 shows the condensation experiments with the s-foil before and after 1 W aging. Visually, the behaviour of the s-foil after 1 W, 1 M, 3 M, 6 M are all similar. In the movie S2, for the 1 W aged sample, one first observes the preferential nucleation of droplets at specific locations, in contrast to the first observation before outdoor tests (movie S1). This phenomenon is due to a memory condensation phenomenon<sup>24</sup>, where water droplets preferentially nucleate at the place where former droplets have evaporated and concentrated deposited aerosols. Concerning the latency time for droplet shedding, the 1 W - aged s-foil exhibits a larger time than the one before aging, in agreement with the former study on repeatability. Figure 4a shows an increase of the latency time with aging. The measurements of contact angle (CA) and contact angle hysteresis (CAH) on the s-foil in its initial state and after 3 months and 6 months aging show that the contact angle varies with aging: initially, CA= 80° and at 6 months aging, CA= 95°. In addition, the CAH goes from 36° to 56° at 3 months aging and finally to 74° at 6 months aging. The increasing shedding time is not only concerned with the loss of surface surfactant but also due to an enhanced surface roughness, which increases the CAH (see movie S2 where the water droplet pinning is stronger on the aged sample). The origin of the enhanced roughness, at the origin of a larger CAH, is related to UV degradation, dust deposition and/or abrasion. The gradual depletion of the food-proof surfactant is caused by repeated dew condensation and rain events.

**$\mu$ -foil study.** The movie S3 presents the condensation experiments for the  $\mu$ -foil sample before aging and after 1 week aging. In both cases one observes the filling of the grooves before large droplets form on the surface. While such large droplets appear only at the bottom of the sample in the initial condensation experiment, they form sooner at different locations with the aged sample. The difference in behaviour lasts only a few minutes; later both samples behave in a similar fashion with the presence at the bottom of the samples of large droplets continuously filled by the micro-channels. The initial difference has to be attributed to aging effects also observed on the s-foil (increase of CAH). Nevertheless, the start of water collection at the bottom of the sample (Figure 4b) is not affected by aging; both samples begin to collect water at similar times. Based on the movie of the experiments one notes that the behaviour of the  $\mu$ -foil after 1 W, 1 M, 3 M or 6 M are all similar. From Figure 4b it appears that the time for droplet shedding does not evolve with the aging time. Because the material is the same, the evolution of the CA and CAH with aging time for the  $\mu$ -foil at a scale lower than the patterning is the same as the s-foil (reported in section s-foil study). CA and CAH at a larger scale are not appropriate because the collection of the condensed water does not involve the formation of droplets on several grooves and their shedding; it is instead the filling of the micro-grooves that matters, where CA and CAH are only involved at the very beginning of the groove filling process when micro-droplets coalesce inside the grooves.

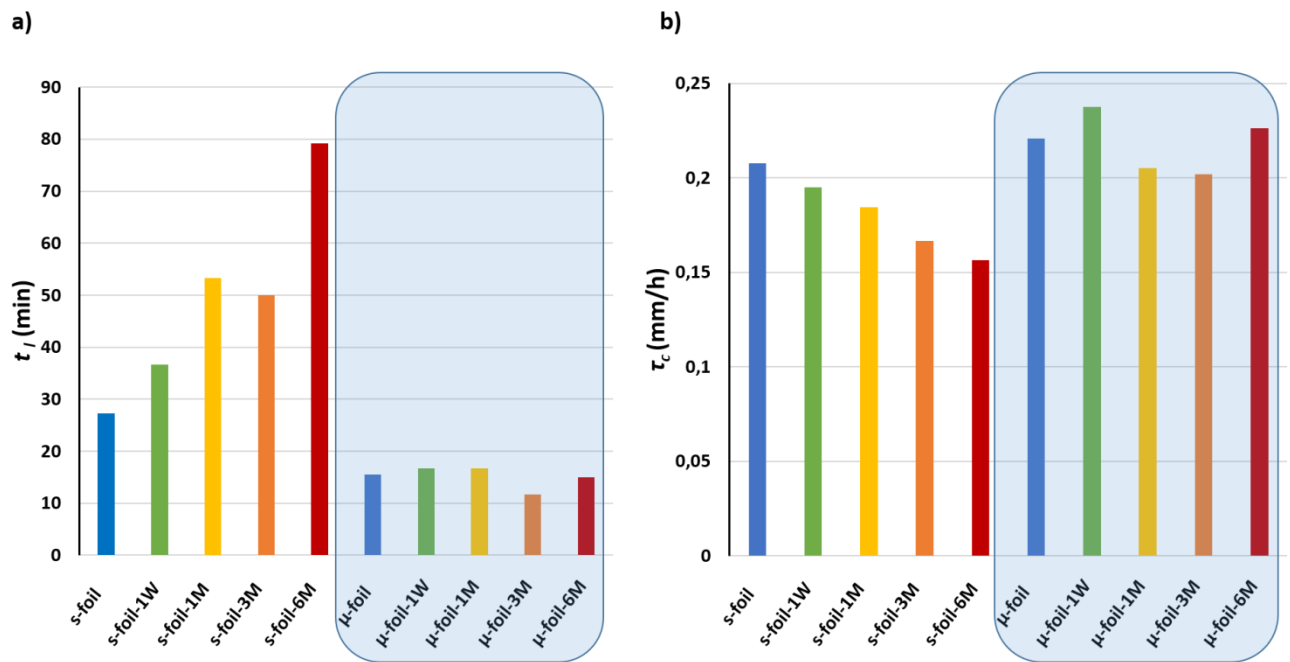
In Figures 4a and 4b the evolutions of the condensation curve before and after aging are different for the s- and  $\mu$ -foils. Concerning the s-foil, before aging (movie S1), the evolution is smooth, in agreement with the presence of the frequent detachment of droplets and the existence of many rivulets (movie S1). However, when the foil is aged, one observes many small jumps in the evolution. These jumps correspond to the less frequent detachment of larger drops inducing less frequent rivulets. The critical drop radius for shedding is indeed proportional to  $CAH^{17}$ , whose value increases with aging. The inset of Figure 4a focuses on the first 5000 s of the experiments. One observes an increase of the latency time for water collection with the aging time. Concerning the  $\mu$ -foil, the inset of Figure 4b shows that the latency time for water collection is not impacted by aging. Additionally, all condensation curves of Figure 4b remain smooth, in agreement with the observations in the movies of many drops continuously detaching from the bottom of grooves filled with water.



**Figure 4: Water collection capability with outdoor aging.** Evolution of the mass of the collected water for s-foil (a) and  $\mu$ -foil (b) prior aging and after 1 week (1 W), 1 month (1 M), 3 months (3 M) and 6 months (6 M) outdoor aging. The insets focus on the beginning of the experiments. The latency time,  $t_l$ , represents the time needed to collect the first droplets.

Figures 5a and 5b displays the evolution with aging of the latency time ( $t_l$ ) for water collection and the collection rate ( $\tau_c$ , defined as the volume of collected water per surface area and time) for the s- and  $\mu$ -foil samples. The latency time increases with aging time for s-foil from 27 to 80 minutes, whereas this time does not significantly evolve for the  $\mu$ -foil, with an average value of 15 minutes. A decrease of  $\tau_c$  with aging time is measured for the s-foil, from 0.21 to 0.16 mm/h. This decrease should correspond to the increase of the critical size for droplet shedding (as measured by the evolution of the CAH with aging), which increases the thermal resistance. (Note that this thermal effect and thus the lowering of condensation rate should not occur under outdoor radiative cooling where water cools very efficiently due to its high

emissivity). In contrast, no significant evolution with aging is observed with the  $\mu$ -foil within experimental variations ( $\mu$ -foil-3M). These variations can be attributed to corresponding variations in supersaturation alike the  $\mu$ -foil-1 set in Fig. 1c. This is because, as already noted, the water collection is limited by the filling of the grooves and not impacted by the CAH increase. The measurements of these parameters indicate that the s-foil is largely impacted by aging, whereas the  $\mu$ -foil is not. This significant result indicates that the micro-structures prevent aging. After 6 months aging,  $\mu$ -foil exhibits a latency time of almost an order of magnitude less than the s-foil and displays a collection rate larger by near 50%.

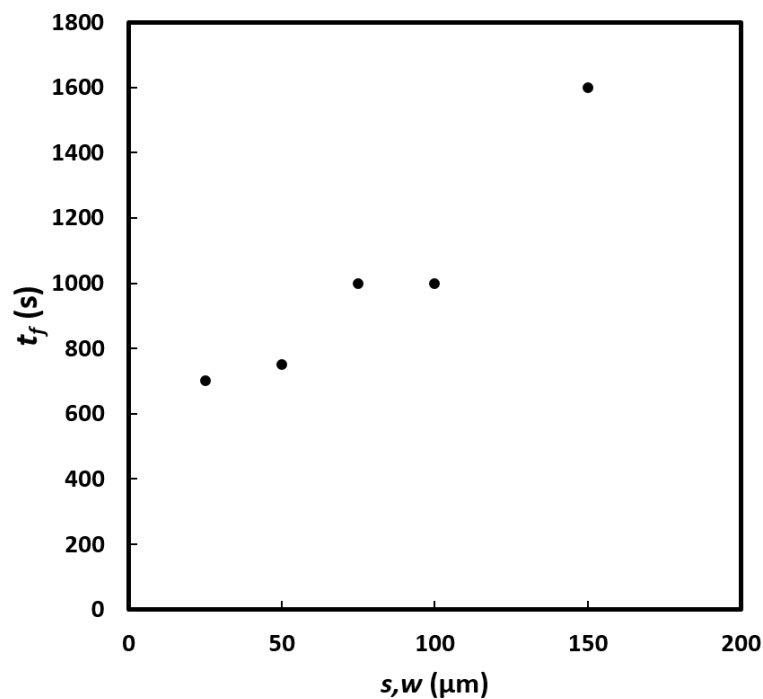


**Figure 5: Water collection capability for s-foil and  $\mu$ -foil with outdoor aging:** (a) Latency time for first droplet collection,  $t_l$ , in min. and (b) collection rate,  $\tau_c$ , expressed in volume of the collected water per surface area and time prior material aging and after 1 week (1 W), 1 month (1 M), 3 months (3 M) and 6 months (6 M) outdoor aging.

Although the process of condensation in micro-grooves have been studied in earlier publications<sup>14–16</sup>, we now present a condensation experiment on micro-grooved silicon wafers (noted as  $\mu$ -Si) to better understand the mechanism of water collection inherent to the micro-grooves. Silicon is a material where visualization under an optical microscope is easy, in contrast with the white  $\mu$ -foil (see movie S4). The movie S5 presents a condensation experiment on  $\mu$ -Si with typical grooves dimensions  $s = w = 25 \mu\text{m}$ ,  $d = 50 \mu\text{m}$ . It is first observed that condensation takes place on the top plateaus surfaces, with almost no water seen at the bottom of the grooves due to a lower supersaturation as a result of cavity-edge effects<sup>25</sup>. Droplets then grow by direct accretion of water molecules and by coalescence on the top of the plateaus, until their size is comparable to the width of the plateaus, i.e.  $25 \mu\text{m}$ ; droplets

then move into the grooves by capillary effects and slowly fill them while condensation still takes place on the plateaus. The droplets formed at the top of the plateau coalesce with the filled channels with time, until a complete filling is achieved. Dividing by two the dimensions of  $s$ ,  $w$  with respect to the dimensions of the  $\mu$ -foil grooves does not alter the mechanism as outlined below and allows a faster filling of the grooves to be made. Large droplets, as observed in movies S1 or S3, form at the bottom of the sample, attached to several grooves that continuously supply them with water. This collection mode is inherent to the presence of grooves. The time needed to fill all channels is directly correlated to the time of formation of the major droplets; indeed, major droplets at the bottom of the sample form when all channels are filled with water. The formation of the major droplets is also directly correlated to the latency time for water collection, as these droplets detach and are absorbed by the tissue placed at the bottom of the sample.

In order to study the impact of the dimensions of the channels on the time needed for the complete channels filling ( $t_f$ ), micro-grooved silicon wafers of characteristic sizes  $s = w = 25, 50, 75, 100$  and  $150 \mu\text{m}$  ( $d = 50 \mu\text{m}$ ) were studied. Figure 6 reports the time needed to fill the channels as a function of  $s$  and  $w$  at constant  $d = 50 \mu\text{m}$ . A linear dependency is observed, a decrease of the plateau and groove thickness  $s$  and  $w$  obviously decreasing the filling time of grooves of constant depth. This result indicates that the latency time for water collection can be adjusted and reduced by tuning the characteristic size of the micro-grooves. Additionally, the size of the grooves should also impact the global, long-term, water collection ability (collection rate,  $\tau_c$ ) of the surface<sup>20</sup>.



**Figure 6: Impact of micro-grooves characteristic sizes on water collection ability:** Evolution of the grooves filling time ( $t_f$ ) as a function of the micro-grooves spacing ( $s$ ) and width ( $w$ ) ( $s=w$ ,  $d= 50 \mu\text{m}$ ) on silicon.

## Conclusions:

Outdoor aging involves a surface to be exposed to severe hot and cold temperature conditions, UV degradation, wind and dust abrasion, dust deposition and water exposure. The surface properties are thus challenged with such outdoor conditions, which drive the evolution of the thermal, wetting and adhesive properties of the surface. There is thus a need to engineer robust surfaces, able to handle with severe outdoor conditions. The engineering of surface micro-grooves on foil is an answer to this concern where the surface becomes nearly insensitive to its wetting and roughness characteristics, both properties that evolves with aging. No aging effect will thus appear as long as condensed water remains collected through the micro-channels continuously filled by droplet coalescences from the top plateaus. This collection mode, depending on surface geometry, enables an efficient, sustainable and robust water collection. The two key parameters, the latency time for droplet collection and the collection rate, were shown to be unaffected by aging (even after a rainy sand storm). Furthermore, the ability of the micro-grooved sample to rapidly collect condensed water under various supersaturations indicates a successful operating surface under various climatic conditions. Additionally, surface emissivity and albedo were not significantly impacted with aging, which highlights the robustness of the  $\mu$ -foil passive cooling properties over time.

Passive dew collectors based on radiative cooling have the potential to collect dew water in regions where the dew point temperature is easily reached at night ( $\text{RH} > 70\%$ ). The theoretical maximal yield for dew collection under these conditions is on the order of  $1 \text{ L}\cdot\text{m}^{-2}$  per night<sup>26</sup>. However, these dew events strongly depend on meteorological conditions. Hence, large collecting surfaces are needed implying scalable and low-cost technologies. The present LDPE-based foil price is approximately one euro per square meter and hot embossing is a cheap technology for micro-grooving. In addition to the low-tech and scalable properties, the materials need to be sustainable towards aging, which was addressed by surface geometry. Recycling possibilities also need to be considered, the presented material, which is mostly made of LDPE, is recyclable.

## Materials and methods:

### *Sample preparation:*

Low density polyethylene (96% vol.) (foil) was embedded by microbeads of  $\text{TiO}_2$  and  $\text{BaSO}_4$  and a food-proof surfactant was added to form s-foil (total additives 4% vol.). Micro-grooves of characteristic sizes ( $s=w=d= 50 \mu\text{m}$ ) was engineered on the surface of 0.3 mm thick foil foils by hot embossing at  $98^\circ\text{C}$  under 50 kN force during 90 minutes to produce the  $\mu$ -foil. Hot

embossing is achieved using a nickel mold obtained by electroplating on a 5-inch silicon wafer embedding a thin silver layer acting as the seed layer and lithography-defined micro-patterns of SU8 photoresist (Kayaku Advanced Materials). The s-foil and  $\mu$ -foil samples were cut to  $9 \times 9$  cm<sup>2</sup> dimensions before testing. The  $\mu$ -Si silicon samples were produced from single-side polished [100]-oriented silicon wafers of 4-inch breadth and 525  $\mu$ m thickness (from Siltronic) with a resistivity of 1–20  $\Omega$ cm. The fabrication of the silicon micro-grooves is carried out in a A601E Alcatel plasma etch tool configured for Deep Reactive Ion Etching process (DRIE)<sup>27</sup>. Etching of the 50  $\mu$ m-deep micro-grooves with vertical sidewalls is achieved by alternating plasma etching and passivation steps under SF<sub>6</sub> and C<sub>4</sub>F<sub>8</sub>, respectively, on the lithography-defined patterns leading to the  $\mu$ -Si of characteristic sizes ( $s=w= 25, 50, 75, 100$  or  $150$   $\mu$ m and  $d= 50$   $\mu$ m). The  $\mu$ -Si samples were cut into  $2 \times 2$  cm<sup>2</sup> squares before testing.

#### *Aging conditions:*

Two  $9 \times 9$  cm<sup>2</sup> samples of s-foil and  $\mu$ -foil were set on a 30° tilted planar support oriented South-West on a terrace elevated at around 20 m from the ground floor in Paris (5<sup>th</sup> arrondissement). The overall test duration was 6 months, between 17/02/2022 and 17/08/2022. Outside temperatures were measured between 0.2°C and 39.7°C, with several heat waves. The wind speed was measured between 0 and 20.5 m/s, with several episodes of storm, of which one rainy sandstorm mid-April, 2022. The samples were removed from aging location for condensation testing after 1 week (1 W), 1 month (1 M), 3 months (3 M) and 6 months (6 M).

#### *Condensation in climatic chamber – Collected water volumes:*

Condensation was performed on  $9 \times 9$  cm<sup>2</sup> s-foil and  $\mu$ -foil samples prior aging or at different times of outdoor aging, placed at 90° from horizontal on a vertical Peltier thermostat in a climatic chamber (Weiss, WKL 100) with controlled temperature (at 30°C) and relative humidity (50, 60 or 70%). The Peltier element was working at 3.8 V and 2.5 A (generator, TTI QPX 1200L) and cooled by water controlled at 10°C (Julabo F250) in order to maintain its surface temperature at 16°C. Substrates temperatures were recorded by using thermocouple sensors and the software Picolog. Condensation was observed using a video camera (Imaging Source, DFK 23U445) with a recording time of 1 image every 10 s. Water droplets were collected by a hydrophilic stamp placed at 0.1 mm from the bottom of the studied samples. The stamps were mounted on a balance (Denver Instrument, SI-603, accuracy of 1 Mg), with data recorded every 2 s by using a MATLAB code. Experiments were performed for about 4 h.

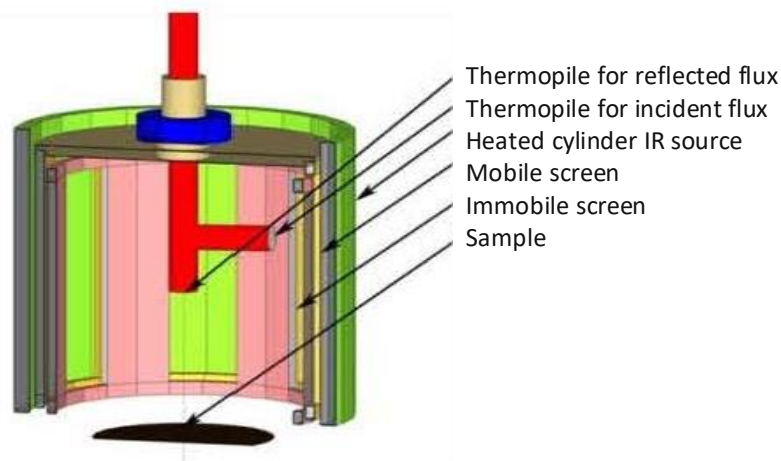
#### *Condensation under microscope:*

Condensation was performed on  $2 \times 2$  cm<sup>2</sup>, horizontal  $\mu$ -foil or  $\mu$ -Si samples in a home-made mini-climatic chamber mounted on an optical microscope (Leica DMRXE) equipped with a

camera (Imaging Source, DFK 23U445). The mini-climatic chamber is composed of (i) a Peltier thermostat for conductive cooling, on which is placed the samples, (ii) a polystyrene cover to hermetically lock the samples with a top opening for a sealed glass slide for optical observation, four side openings for the entrance and exit of saturated humid air, (iii) a pump (Rena 101) and tubes are used to inject air in a flask with water in order to re-inject saturated humid air at room temperature (20 °C) to the two side openings of the sealed mini-chamber. The Peltier element was powered with 2 V and 0.5 A (generator, Sodilec SDRI 205) and the hot side cooled by water controlled at 10°C (Heto CBN 8-30 and HMT 200) in order to maintain the surface temperature of the Peltier at 4°C. Surface temperature was monitored by using thermocouple sensors and the software Picolog. The relative humidity in the mini-chamber was 90%. The temperature of the air in the mini-chamber is equal to the room temperature,  $\approx 20^\circ\text{C}$ . The IC Capture software was used for the video sequence acquisition (15 FPS).

### Supplementary Information:

The emissivity measurement is obtained by the apparatus EM3 from THEMACS Engineering<sup>28</sup>. It uses a hemispherical infrared flux radiation source at a temperature very close to the sample temperature (Figure S1). It is modulated by movable shutters at 10 Hz frequency for the cylindrical wall (presence of 6 windows) and 5 Hz for the top part (presence of 3 windows). This modulation method offers the opportunity to separate the steady sample's own flux from the modulated reflected flux. A thermopile measures the flux reflected in a normal direction by the surface of the material and another thermopile measures the IR flux emitted by the source.



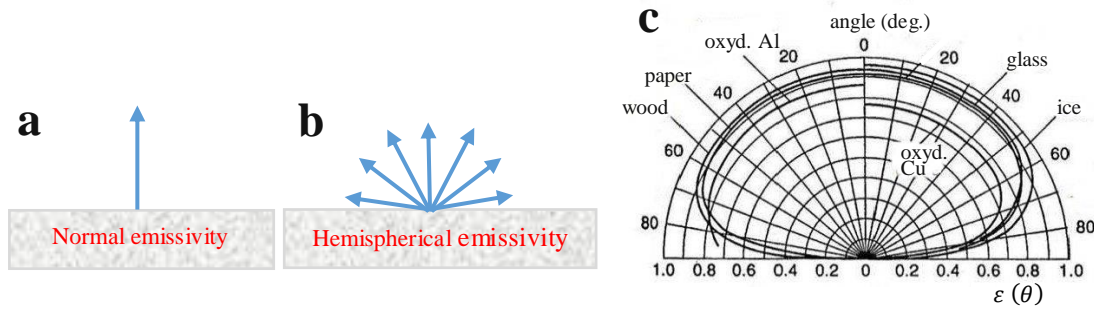
**Figure S1: The setup for emissivity measurements.** (Adapted from Ref. 29).

The ratio of the two measurements (emitted and reflected fluxes) is proportional to the normal reflectivity coefficient  $\rho_N$ . Considering the Kirchhoff's law for an opaque material, the normal emissivity  $\varepsilon_N$  is then obtained by the following relationship  $\varepsilon_N = 1 - \rho_N$ .



In order to consider the IR emission in all directions as illustrated in Figure S2, the hemispherical emissivity is defined by the expression, where  $\theta$  and  $\varphi$  are the angles of the emission with respect to the normal at the surface and  $\varepsilon(\theta, \varphi)$  the directional emissivity:

$$\varepsilon_H = \frac{1}{\pi} \int_0^{\pi/2} \int_0^{2\pi} \varepsilon(\theta, \varphi) \cos(\theta) \sin(\theta) d\theta d\varphi$$



**Figure S2:8. Two-dimensional representation of normal (a) and hemispherical (b) emissivity. (c) Directional emissivity for some typical materials. (Adapted from Ref. 30).**

If the directional emissivity cannot be measured for all directions  $\theta$  and  $\varphi$ , one can deduce the hemispheric emissivity from normal directional emissivity by the ratio  $\varepsilon_H / \varepsilon_N = A$ , where  $A$  is a coefficient obtained from the Fresnel equation for reflexion<sup>31</sup>. Standard EN 12898 provides the ratio between the normal and hemispherical emissivities ( $A$  values); it is reported in Table S1. The device is calibrated beforehand using two known reference materials, a low emissive surface (aluminum) and a high emissive surface (Nextel paint, 3M™).

Total emissivity at normal incidence $\varepsilon_N$	0.03	0.05	0.1	0.2	0.3	0.4	0.5	0.6	0.7	0.8	0.89
$A = \varepsilon_H / \varepsilon_N$	1.22	1.18	1.14	1.1	1.06	1.03	1	0.98	0.96	0.95	0.94

**Table S1: Ratio between normal emissivity and hemispherical emissivity.**

### Acknowledgements:

This project was funded by the METAWATER Project (No. ANR-20-CE08-0023 METAWATER). The authors thank F. Marty for the SEM observation and for the preparation of the Si samples in ESIEE cleanroom facilities within the ESYCOM Lab. The authors thank G. Basset (CSEM, Switzerland) for the foil embossing.

### Conflict of Interest:

The authors declare no conflict of interest.

## References:

1. Mekonnen, M. M. & Hoekstra, A. Y. Four billion people facing severe water scarcity. *Sci. Adv.* **2**, e1500323 (2016).
2. Oki, T. & Kanae, S. Global Hydrological Cycles and World Water Resources. *Science* **313**, 1068–1072 (2006).
3. Liu, X., Beysens, D. & Bourouina, T. Water Harvesting from Air: Current Passive Approaches and Outlook. *ACS Materials Lett.* **4**, 1003–1024 (2022).
4. Beysens, D. *Dew water*. (River Publishers, 2018).
5. Kabela, E. D., Hornbuckle, B. K., Cosh, M. H., Anderson, M. C. & Gleason, M. L. Dew frequency, duration, amount, and distribution in corn and soybean during SMEX05. *Agricultural and Forest Meteorology* **149**, 11–24 (2009).
6. Preston, D. J. *et al.* Heat Transfer Enhancement During Water and Hydrocarbon Condensation on Lubricant Infused Surfaces. *Sci Rep* **8**, 540 (2018).
7. Sun, J., Jiang, X. & Weisensee, P. B. Enhanced Water Nucleation and Growth Based on Microdroplet Mobility on Lubricant-Infused Surfaces. *Langmuir* **37**, 12790–12801 (2021).
8. Wang, D. *et al.* Design of robust superhydrophobic surfaces. *Nature* **582**, 55–59 (2020).
9. Hoque, M. J. *et al.* Life Span of Slippery Lubricant Infused Surfaces. *ACS Appl. Mater. Interfaces* **14**, 4598–4611 (2022).

10. Peppou-Chapman, S., Hong, J. K., Waterhouse, A. & Neto, C. Life and death of liquid-infused surfaces: a review on the choice, analysis and fate of the infused liquid layer. *Chem. Soc. Rev.* **49**, 3688–3715 (2020).
11. Bai, H. *et al.* Improved Liquid Collection on a Dual-Asymmetric Superhydrophilic Origami. *Advanced Materials* **35**, 2211596 (2023).
12. Han, T., Choi, Y., Jeong, J., Choi, J. H. & Jo, H. Sustainable thin-film condensation with free surface flow through water film network. *International Journal of Heat and Mass Transfer* **196**, 123222 (2022).
13. Nioras, D., Ellinas, K. & Gogolides, E. Atmospheric Water Harvesting on Micro-nanotextured Biphilic Surfaces. *ACS Appl. Nano Mater.* **5**, 11334–11341 (2022).
14. Al-Khayat, O., Hong, J. K., Beck, D. M., Minett, A. I. & Neto, C. Patterned Polymer Coatings Increase the Efficiency of Dew Harvesting. *ACS Appl. Mater. Interfaces* **9**, 13676–13684 (2017).
15. Lee, A., Moon, M.-W., Lim, H., Kim, W.-D. & Kim, H.-Y. Water harvest via dewing. *Langmuir* **28**, 10183–10191 (2012).
16. Pinheiro, R. A., Silva, A. A., Trava-Airoldi, V. J. & Corat, E. J. Water vapor condensation and collection by super-hydrophilic and super-hydrophobic VACNTs. *Diamond and Related Materials* **87**, 43–49 (2018).
17. Nilsson, T. M. J., Vargas, W. E., Niklasson, G. A. & Granqvist, C. G. Condensation of water by radiative cooling. *Renewable Energy* **5**, 310–317 (1994).
18. Beysens, D., Milimouk, I., Nikolayev, V., Muselli, M. & Marcillat, J. Using radiative cooling to condense atmospheric vapor: a study to improve water yield. *Journal of Hydrology* **276**, 1–11 (2003).

19. Trosseille, J., Mongruel, A., Royon, L. & Beysens, D. Effective substrate emissivity during dew water condensation. *International Journal of Heat and Mass Transfer* **183**, 122078 (2022).
20. Bintein, P.-B., Lhuissier, H., Mongruel, A., Royon, L. & Beysens, D. Grooves Accelerate Dew Shedding. *Phys. Rev. Lett.* **122**, 098005 (2019).
21. Narhe, R. D. & Beysens, D. A. Nucleation and Growth on a Superhydrophobic Grooved Surface. *Phys. Rev. Lett.* **93**, 076103 (2004).
22. Guo, Z., Boylan, D., Shan, L. & Dai, X. Hydrophilic reentrant SLIPS enabled flow separation for rapid water harvesting. *Proc. Natl. Acad. Sci. U.S.A.* **119**, e2209662119 (2022).
23. ElSherbini, A. I. & Jacobi, A. M. Retention forces and contact angles for critical liquid drops on non-horizontal surfaces. *Journal of Colloid and Interface Science* **299**, 841–849 (2006).
24. Lavielle, N., Beysens, D. & Mongruel, A. Memory Re-Condensation. *Langmuir* **39**, 2008–2014 (2023).
25. Medici, M.-G., Mongruel, A., Royon, L. & Beysens, D. Edge effects on water droplet condensation. *Phys. Rev. E* **90**, 062403 (2014).
26. Tomaszewicz, M., Abou Najm, M., Beysens, D., Alameddine, I. & El-Fadel, M. Dew as a sustainable non-conventional water resource: a critical review. *Environ. Rev.* **23**, 425–442 (2015).
27. Marty, F. *et al.* Advanced etching of silicon based on deep reactive ion etching for silicon high aspect ratio microstructures and three-dimensional micro- and nanostructures. *Microelectronics Journal* **36**, 673–677 (2005).

28. <https://themacs-engineering.com/en/non-classe/the-em3-emissiometer-produced-by-the-themacs-engineers/>. Accessed on june 26, 2023.
29. Monchau, J.P. & Hameurry, J., Mesure de l'émissivité thermique, *Technique de l'ingénieur*, R 2 747 – 1 -22, (2018).
30. <https://themacs-engineering.com/wp-content/uploads/2020/05/Mesure-de-l%E2%80%99%C3%A9missivit%C3%A9-thermique.pdf>. Accessed on June, 17 2023.
31. Lorrain, P. & Corson, D.R., Champs et ondes électromagnétiques, (Armand Collin, 1979).